

Broadly tunable photon pair generation in a suspended-core fiber

Jonas Hammer,^{1,2,*} Maria V. Chekhova,^{1,2} Daniel R.
Häupl,^{1,2} Riccardo Pennetta,¹ and Nicolas Y. Joly^{2,1}

¹*Max-Planck-Institute for the Science of Light,
Staudtstraße 2, 91058 Erlangen, Germany*

²*Physics Department, Friedrich-Alexander University,
Staudtstraße 2, 91058 Erlangen, Germany*

(Dated: November 5, 2019)

Abstract

Nowadays fiber biphoton sources are nearly as popular as crystal-based ones. They offer a single spatial mode and easy integrability into optical networks. However, fiber sources lack the broad tunability of crystals, which do not require a tunable pump. Here, we report a broadly tunable biphoton source based on a suspended core fiber. This is achieved by introducing pressurized gas into the fibers hollow channels, changing the step index. The mechanism circumvents the need for a tunable pump laser, making this a broadly tunable fiber biphoton source with a convenient tuning mechanism, comparable to crystals. We report a continuous shift of 0.30 THz/bar of the sidebands, using up to 25 bar of argon.

Optical fibers are an ideal platform for the generation of entangled photon pairs (biphotons) via spontaneous four-wave-mixing (FWM), due to their long light-matter interaction length. In particular, solid core fibers offer high effective nonlinearity. However, they typically lack the convenient tuning mechanism present in crystal-based biphoton sources, beside the trivial but costly scheme of tuning the pump wavelength. A limited amount of tuning has been demonstrated by stretching and heating the fiber [1], however, these approaches are limited by fiber damage. Meanwhile, gas filled hollow-core fibers offer broad dispersion tuning, but implementing a biphoton source in these fibers remains a challenging task, due to their low nonlinearity. Here, we combine the high nonlinearity of a solid core fiber with the convenient tuning scheme offered by gas filled fibers, to implement a tunable source of entangled photons. This is achieved by filling the channels surrounding the core of a suspended-core fiber (SCF). SCFs are a class of index-guiding microstructured fibers, where light is guided in a glass core suspended by three glass nano-membranes. SCFs have been used in a variety of applications, ranging from supercontinuum generation [2] to gas absorption spectroscopy [3], or chemical sensing [4].

In FWM, two photons of an incident beam (denoted pump) are annihilated and the energy is transferred to two daughter photons (denoted signal and idler) symmetrically spaced around the pump. The signal and idler frequencies ω_S , ω_I are determined by the

* jonas.hammer@mpl.mpg.de

phase-matching conditions:

$$\Delta\beta = 2\beta(\omega_P) - \beta(\omega_S) - \beta(\omega_I) - 2\gamma P_{\text{Pump}} = 0 \quad (1)$$

$$2\omega_P - \omega_I - \omega_S = 0, \quad (2)$$

where ω_P is the pump frequency and β denotes the propagation constant. Here, we refer to the blue shifted sideband as signal, and the red shifted one as idler. The last term in Eq. 1 corresponds to a non-linear contribution to the phase-mismatch due to cross-phase and self-phase modulation terms. Eq. 2 ensures energy conservation and leads to a symmetric frequency detuning of the two sidebands.

If a seeding beam at either of the sideband frequencies is present, FWM is an entirely classical phenomenon, also known as parametric amplification. It is exploited in fiber-optic parametric amplifiers or oscillators [5, 6]. If no seeding beams are launched, FWM should be described in the framework of quantum mechanics. In this case the process can be thought of as seeded by vacuum fluctuations and produces photon pairs at the sideband frequencies. This has been used as a source of biphotons in dispersion shifted [7, 8], microstructured [9, 10] or polarization maintaining fibers [11]. Recently, optical fiber tapers have gained some popularity as biphoton sources [12, 13]. Fiber tapers exhibit dispersion and guidance properties similar to SCF, however, the additional structure surrounding the light-guidance region makes SCF less prone to damage and environmental influences. A tunable source of bright squeezed-vacuum twin beams based on a FWM process (modulational instability) has been demonstrated in hollow-core fibers [14]. For such a source, tunability of the number of modes has been demonstrated [15] and proposed for further use in a tunable biphoton source [16].

Here, we use a similar tuning principle but apply it to SCF, where the solid core provides a high nonlinearity. First, we demonstrate the continuous tuning of seeded FWM. Using parametric amplification of a broadband infrared seed, we observe a shift of 7 THz for the emitted conjugate near-infrared sideband (~ 17 nm at this wavelength range), when filling the fiber with up to 25 bar of argon. We then demonstrate a fiber biphoton source with very high coincidence-to-accidental ratio (CAR) and tunability over at least 4.6 THz (~ 30 nm measured at the red detuned wavelength).

Our SCF has an effective core diameter of 830 nm, defined by a circle inscribed into the central glass region. For the parametric amplification experiment (Fig. 1a), the pump is a

1.064 μm passively Q-switched laser (1.8 ns pulses, 42 kHz repetition rate). Most of the laser power is used to generate a supercontinuum in a solid core photonic crystal fiber [17] to serve as a seed. The supercontinuum is long-pass filtered (1.15 μm cut-on). Pump and seed are prepared to be co-polarized and overlapping in time and space. Both beams are coupled to a single mode ultra-high NA fiber (UHNA), which is butt-coupled to the ~ 50 cm long SCF inside of a mini gas cell ([18, 19] for technical details). The out-coupling end of the SCF was mounted in a standard gas cell, where the pressurized gas could be introduced.

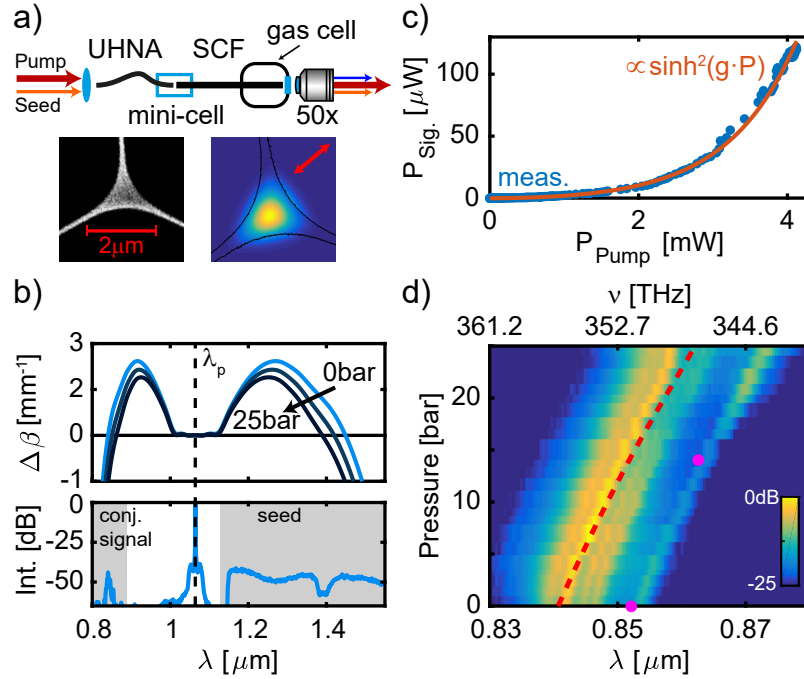


FIG. 1. Seeded FWM. a) Setup for pressure tuning the FWM, see text. The inset shows a SEM of the SCF core-region (left) and a numerical simulation of the fundamental mode of the fiber at 1.064 μm (right, red arrow denotes the polarization) b) Top: Simulated FWM phase-mismatch for the fundamental fiber mode, for increasing the pressure of argon gas filling the the hollow channels of the fiber. Bottom: experimentally measured spectrum after the SCF, when pump and seed are launched into the fiber. c) Pump-power scaling of the signal intensity at constant seed power (blue) and its fit (orange). d) Signal spectrum measured for increasing argon pressures. Red dashed line is an EME-simulation. The two magenta circles mark the conjugate to the wavelengths marked in Fig. 3.

Using an eigenmode expansion (EME), based on a high resolution SEM of the fiber, we

predict a phase-matched FWM signal for the fundamental mode near $0.84 \mu\text{m}$ (Fig. 1b top). The fiber presents two distinct polarization states yielding slightly different phase-matching wavelengths. We choose to work with the polarization parallel to one of the nano-membrane (inset in Fig. 1a, red arrow marks the direction of the polarization). The corresponding phase-matched signal at $\sim 0.84 \mu\text{m}$ (Fig. 1b, bottom) serves as a reference in order to optimize the coupling of the fundamental mode and the polarization states of the pump and seed as well as their time overlap. We also performed near-field imaging of the different wavelengths exiting the SCF, as well as polarization analysis of the fields to confirm that the process indeed only involves one fiber mode [19]. The signal intensity depends on the pump power (Fig. 1c) as $\sinh^2 G$ [20], where $G = g \cdot P_{\text{pump}}$ is called the parametric gain. From the fit we find $g_{\text{avg}} = 0.54 \text{ mW}^{-1}$ in terms of the pump average power ($g_{\text{PP}} = 0.0414 \text{ W}^{-1}$ for peak power [19]).

Filling the SCF hollow channels with argon decreases the frequency detuning of the sidebands, as the argon pressure increases (Fig. 1b, top). This is because the evanescent decay length of the mode into the hollow channels scales with the wavelength. Therefore, the increasing gas refractive index (due to increasing gas pressure and therefore density) affects the propagation constant of the idler more strongly than the signal. This tuning mechanism has been used to shift the resonant third harmonic generation (THG) wavelength in sub-micron tapers [21].

By increasing the pressure from 0 to 25 bar, we observed a continuous shift in the signal wavelength by about 17 nm ($\sim 7 \text{ THz}$) towards smaller detuning (Fig. 1d). The red dashed line corresponds to an EME-simulation. The slight deviation of the simulation from the measured data is mainly due to the neglected chromatic dispersion of the filling gas, an assumption that breaks down at higher gas pressures when chromatic dispersion effects become comparable to the increase in refractive index due to increasing gas density. Fitting the experimental peak-wavelength of the signal spectrum with a first order polynomial yields an average tuning rate of 0.70 nm/bar (0.30 THz/bar). We note that dispersion tuning in SCF has also been demonstrated by depositing a nanofilm on the exposed core [22], however this mechanism is not reversible in contrast to the gas-pressure filling.

We now consider the spontaneous FWM regime, and demonstrate the effect of the gas pressure on biphoton generation. For these experiments the pump was a $1.064 \mu\text{m}$ continuous wave (CW) laser and no seeding was used. The pump was launched in the same polarization

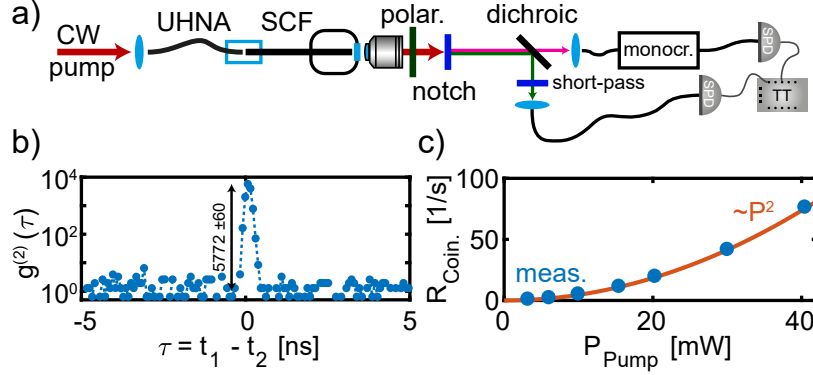


FIG. 2. Spontaneous FWM. a) Experimental setup for measuring two-photon coincidences. A CW-pump at $1.064 \mu\text{m}$ is launched into the UHNA-SCF device. After re-collimation, light passes through a polarizer and the pump is suppressed using a notch filter. Signal and idler photons are split on a dichroic mirror. Signal photons pass through another set of interference filters, and are coupled to a single-photon detector (SPD). Idler photons pass through a monochromator and are then sent to another SPD. Both SPDs are connected to a time-tagger. b) Measured second-order correlation function. c) Measured coincidence rate for increasing pump powers. Orange line is a quadratic fit.

state as found optimal in the previous experiments (Fig. 2a). At exit from SCF, light passed through a polarizer to select the desired polarization state. The pump was suppressed by a notch filter (-60 dB), and the sidebands were split on a dichroic mirror. Signal photons passed through another set of interference filters (short pass, $0.9 \mu\text{m}$ cut off) to further suppress the pump, and were then fiber-coupled to a superconducting nanowire single-photon detector (SPD). Idler photons were directed to a fiber-coupled, home-built grating monochromator, and sent to another SPD. The passband width of the idler monochromator was $\sim 3 \text{ nm}$. The SPDs were connected to a computer-controlled time-tagger, registering single photon events in either signal or idler channel, as well as coincidences between the two. We used a coincidence resolution time (bin-width) $T_b = 80 \text{ ps}$ for the experiments. Pair generation was characterized by measuring the normalized second-order correlation function (Fig. 2b), calculated as

$$g^{(2)}(\tau) = \frac{R_{\text{coin}}(\tau)}{R_S R_I T_b}, \quad (3)$$

where $R_{\text{coin}}(\tau)$ denotes the coincidence rate at a given time delay between two events $\tau = t_1 - t_2$ and $R_{S,I}$ are the count rates of signal and idler detectors respectively. The pump power

was 10 mW coupled to the fiber, and the monochromator was set to $1.46 \mu\text{m}$. The peak value of $g^{(2)}$, sometimes called coincidences-to-accidentals ratio (CAR), is 5770 ± 60 . Outside of the central peak, $g^{(2)}(\tau)$ drops to unity -i.e. only accidental coincidences are detected [23]. For lower pump powers we measured even higher values of the CAR exceeding 10^4 [19]. In Fig. 2c the measured maximum coincidence rate [i.e. the value of $R_{\text{coin}}(\tau = 0)$] is shown as a function of the coupled CW pump power. This includes detection and coupling losses after SCF. The fit in Fig. 2c is a parabola, corresponding to the low gain expansion of the theoretical power scaling. Through comparison with the previously found value of g_{PP} we can estimate the parametric gain as $G \approx 4 \cdot 10^{-4}$ at 10 mW pump power.

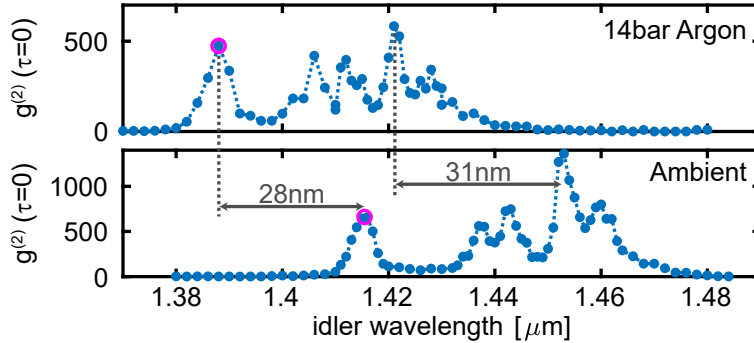


FIG. 3. Tuning of spontaneous FWM. Peak value of the second-order correlation function measured versus the idler wavelength for SCF at ambient pressure (bottom) and filled with 14 bar argon (top). The spectral features shift by about 30 nm. The two magenta circles are the idler wavelengths corresponding to the marked wavelengths in Fig. 1.

To study the effect of gas-pressure tuning on the spontaneous FWM we performed a set of measurements, where the SCF was either in air (ambient pressure) or filled with 14 bar of argon. In each measurement the pump power was 20 mW, and we scanned the monochromator across the spectral region where biphoton emission is expected. At each monochromator setting we collected data for 60s. The CAR versus the monochromator setting is shown in Fig. 3, for the case of air and 14 bar argon in the SCF. Similar to the seeded case, with increasing argon pressure the emission spectrum shifted to smaller detunings with the same tuning rate ($\sim 0.3 \text{ THz}/\text{bar}$).

The $g^{(2)}$ spectrum demonstrates features very similar to those obtained in the seeded case. In particular, the two magenta markers in Fig. 3 correspond to the conjugates of the signal

wavelengths that were marked in Fig. 1c at the same pressures. The normalized second-order correlation function measured at 14 bar is slightly reduced compared to the measurement at ambient pressure, possibly due to a higher parametric gain and higher count rates.

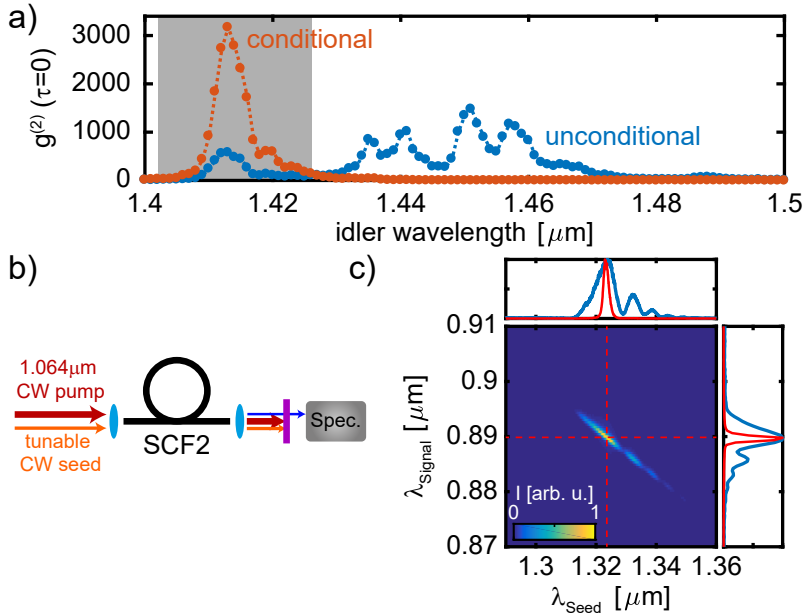


FIG. 4. Frequency entanglement. a) Peak value of $g^{(2)}$ as a function of the monochromator wavelength measured at ambient pressure. For the unconditional measurement (blue) the signal photons are unfiltered, whereas for the conditional measurement (orange) a bandpass filter ($0.85 \mu\text{m}$) is inserted in front of the signal SPD. The grey box corresponds to the conjugate of the $0.85 \mu\text{m}$ bandpass full width at half maximum region. b) Setup for a stimulated emission tomography (SET) measurement of SCF2 (different phasematching point compared to SCF used before, length $\sim 12 \text{ cm}$). c) SET measurement result (heatmap). The line plots (top and right) are the marginal distributions (blue) and cuts along the dashed lines (red).

We verified the frequency entanglement of the photon pairs comparing conditional and unconditional two-coincidence measurements. In Fig. 4a the peak value of $g^{(2)}$ is plotted as a function of the monochromator wavelength, the experimental conditions were similar to the ambient case in Fig. 3. The blue dots in Fig. 4a correspond to a measurement where all signal photons are directed to the SPD (unconditional measurement). The orange dots correspond to a conditional measurement, i.e. only photons of a specific wavelength ($0.85 \mu\text{m}$) reach the signal SPD. The spectrum of coincidences is much narrower in this scenario, a typical sign for frequency entanglement of the photon pairs [24, 25].

Additionally we performed a stimulated emission tomography (SET) measurement. SET retrieves the joint spectral intensity (JSI) of a biphoton source by launching the pump alongside a narrowband tunable seed to the system [26, 27]. To match the tuning range of our seeding laser (telecom O-band, ~ 40 MHz linewidth), we used a fiber with slightly smaller effective core diameter and therefore smaller frequency detuning, we denote the fiber SCF2. The fiber shows otherwise very similar properties. The SET setup is shown in Fig. 4b, pump and seed (both CW and co-polarized) are launched into SCF2. At exit from the fiber seed and pump are blocked and only the conjugate signal is recorded on a CCD-spectrometer. The JSI is retrieved by scanning the tunable laser across the phase matching point (Fig. 4c). From the JSI we can confirm a high degree of frequency entanglement. The marginal distributions (blue line plots) and the cuts through the JSI (red line plots) correspond to unconditional and conditional measurements at the respective cross-section.

Finally we want to note that the overall shape of the emission spectra measured from our SCF are due to inhomogeneities of the fibers, which we confirmed via cutback measurements. We estimate a deviation of ± 2.5 nm of the effective core diameter over a fiber length of ~ 50 cm [19]. This could be potentially improved during fiber fabrication, or by careful selection of a shorter fiber piece with less fluctuations. The overall principle of our tuning mechanism etc. is, however, not affected by this.

In conclusion, we have demonstrated a tunable source of entangled photons, in which the spontaneous emission spectrum can be shifted by 0.70 nm/bar on the signal side by changing the pressure of the filling gas (argon). Our method allows tuning over a wide range of wavelengths, limited only by the maximum achievable refractive index of the filling gas. For the SCF in our experiments we estimate a sideband shift of ~ 40 THz (840 nm to 950 nm) when filling the fiber with up to 45 bar of Xenon. In the seeded case such a system might be used to implement an all-fiber tunable parametric amplifier. The use of a solid core, small mode area fiber facilitates the use of low-power pump lasers, which may be of interest for small-footprint devices. Furthermore, the same principle could be used for tuning the phase matching of FWM or parametric down-conversion in other types of exposed core waveguides, e.g. on-chip ridge waveguides.

We acknowledge funding by Deutsche Forschungsgemeinschaft (DFG) (CH-1591/3-1, JO-1090/3-1), and the Max Planck School of Photonics.

SUPPLEMENTAL MATERIALS

1. Parametric gain

The maximum parametric four-wave-mixing (FWM) gain, at the phase-matching point is calculated as [20]:

$$G_{\max} = \gamma P_{\text{Peak}} L, \quad (4)$$

With the pump peak power P_{Peak} , the fiber length L and the nonlinear parameter $\gamma = n_2\omega(A_{\text{eff}}c)^{-1}$. Here n_2 is the nonlinear refractive index of silica and c the speed of light. From the eigenmode expansion simulation (EME) we calculate the effective mode area as

$$A_{\text{eff}} = \frac{(\iint |F|^2)^2 dx dy}{\iint |F|^4 dx dy}, \quad (5)$$

with F describing the electric field distribution of the mode. As an approximation we evaluate the nonlinear parameter at the pump frequency only and find $\gamma = 0.16 (\text{m} \cdot \text{W})^{-1}$. The gain g_{PP} is obtained from γL ($L = 50 \text{ cm}$), which yields $g_{\text{PP}} = 0.08 \text{ W}^{-1}$, close to the value extracted by fitting the experimental data (0.04 W^{-1}). The values g_{PP} and g_{avg} are related by the duty cycle of the pump laser: $g_{\text{avg}} = g_{\text{PP}}(\tau F_{\text{rep}})^{-1}$. Accordingly, $g_{\text{avg}} = g_{\text{PP}}$ for the case of a CW pump.

2. Polarization dependence of the phase-matching

From EME-simulations we predict a resonant FWM signal near $0.84 \mu\text{m}$ for the fibers fundamental mode. The two polarization states (denoted A and B) are non-degenerate (see Fig. 5b and c for the near field and FWM phase-mismatch of both polarization modes). We used the setup shown in Fig. 5a to characterize the modes: the co-polarized pump and seed collectively pass through a half-wave-plate and are coupled to a $\sim 40 \text{ cm}$ long suspended core fiber (SCF), at exit from SCF light passes through a polarizer and is steered to a spectrometer. Note: this experiment was carried out using a piece of the SCF not attached to the mini-cell (as in the main paper), to have a more precise control over the polarization.

The bottom plot in Fig. 5c shows the spectrum of the fiber output for two orthogonal settings of the read-out polarizer. The pump average power was 0.5 mW , and spectra were

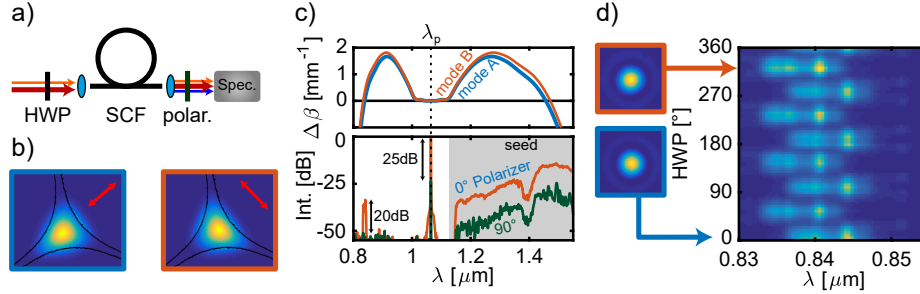


FIG. 5. a) setup to characterize the polarization dependence of the phase-matching. b) simulated near fields of the two polarization states of the fiber fundamental mode. c) FWM phase-mismatch for the two polarization states (Top). Bottom shows the experimental spectrum when all light is launched into the polarization state denoted *mode B*, when the read out polarizer is set to maximize the signal (orange) or rotated 90° (green). d) spectrum of the conjugate signal recorded for varying settings of the input half-wave-plate (HWP), read-out polarizer removed. Insets show experimental near field images of mode A and B.

recorded using an optical spectrum analyzer (OSA). The HWP before the fiber was adjusted to maximize the signal around $0.840 \mu\text{m}$. Comparing the two measurements and taking into account the simulated FWM phase-matching condition confirms that all fields are co-polarized and guided in the same fiber mode. Note that the -25 dB pump suppression corresponds to the performance characteristic of the broadband polarizer, and the -20 dB suppression of the signal is a lower bound because of the OSA noise floor. Rotating the HWP in front of the fiber (read-out polarizer removed) revealed two distinct sets of resonant wavelengths, corresponding to the polarization states A and B, see Fig. 5d. We can infer that the peak in Fig. 5c corresponded to mode A, which is resonant at smaller detuning. The near field images in Fig. 5d were recorded using bandpass filters to block seed and pump. Due to the sub-micron size of the modes we cannot optically resolve the tiny difference of the two polarization states predicted by the EME. The faint halo around the modes is an artifact of the imaging system.

3. Shape of the emission spectrum

The FWM-emission spectra (seeded and spontaneous) of the fibers in use often show more than one dominant peak. We performed a cutback measurement of a piece of SCF to

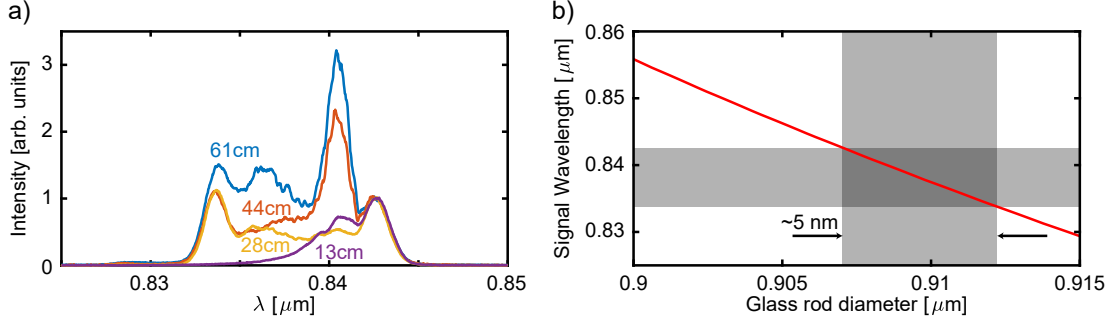


FIG. 6. a) Seeded FWM signal spectrum measured during a cutback. Spectra are normalized to the peak on the long wavelength side. b) FWM-signal wavelength for a silica-glass rod in air vs glass rod diameter. This shows similar dispersion properties to the SCF. The horizontal shaded box corresponds to the spectral region where peaks are observed in a. We infer that the SCF effective core diameter varies by about ± 2.5 nm.

investigate the origin of this structure, and found that it is related to the (in-)homogeneity of the fiber.

In Fig. 6a we present the conjugate signal spectrum measured in seeded FWM, when cutting back a 61 cm length of the SCF. During the cutback we can observe peaks vanishing from the spectrum, hinting towards fiber inhomogeneity as the origin of the multi peak structure. From the measurement we can estimate that from our particular fiber we can get close to 20 cm of fiber without a prominent multi peak structure (for example the peak around 0.84 μm almost completely vanishes when cutting from 44 cm to 28 cm).

To estimate the amount of fiber diameter variation to cause this spectrum, we modeled the fiber as a cylindrically symmetric glass rod in vacuum and calculate the resonant signal wavelength as a function of the glass rod diameter [28]. Comparing the observed range of signal wavelength emission with the calculation, we can estimate that the SCF effective core diameter exhibits inhomogeneities on the order of ± 2.5 nm over the length of the cutback.

4. Mini gas cell

We used the setup sketched in Fig. 7 as an experimentally convenient way to couple light into the sub-wavelength sized core of the SCF. The setup is based on the scheme presented in reference [18]. Light is coupled to an ultra high NA (UHNA) fiber (mode

field diameter $\sim 2.6 \mu\text{m}$), which is butt-coupled to the SCF inside of a mini gas cell. The resulting coupling efficiencies (including free-space coupling to the UHNA fiber) are typically $\sim 30\%$. The end of the UHNA fiber and the in-coupling side of SCF are each glued into thick-walled capillaries, providing mechanical stability. The mini cell was fabricated on a standard fiber launching stage such that capillary-1 (UHNA) was fixed and capillary-2 (SCF) could be moved to optimize the coupling. These capillaries are then glued into a thin-walled capillary, forming the outside of the mini cell. During the curing process of the glue in this step, the transmission was monitored and coupling was optimized until the glue had set.

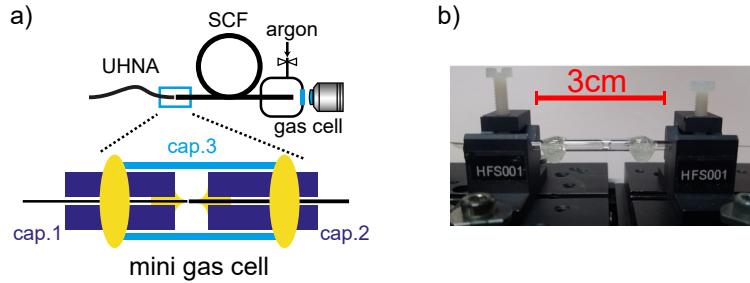


FIG. 7. a) Detailed sketch of the mini-cell for coupling the ultra high NA (UHNA) fiber to the SCF. The mini cell is made up of three glass capillaries (cap.1-3) . Gas is introduced via the standard gas cell with a window for out-coupling. b) Picture of the mini-cell.

The out-coupling end of the SCF was mounted in a standard gas cell, where the pressurized gas could be introduced. Light emerging from the gas cell was collimated using a 50x objective with a long working distance. The small volume ($V \approx 12 \text{ mm}^3$) of the mini-cell was filled up via the SCFs hollow channels. Depending on the desired change in filling pressure this can take several minutes, however we found that the pressure independent coupling to a precisely defined fiber mode obtained in this way drastically facilitates experiments. The scheme could potentially be extended to have the mini cell on each fiber end, and directly introducing the gas into one or both of the mini cells via some extra port on capillary-3.

5. Coincidence to accidental ratio

In Fig 8 we provide a measurement of the second order correlation function $g^{(2)}(\tau)$ for low pump power (0.8 mW CW) and a bandpass filter/monochromator inserted on both signal

and idler arms respectively. Data was recorded for 3.5 h, coincidence bin width was 80 ps. We estimate a CAR value of 15400 ± 500 .

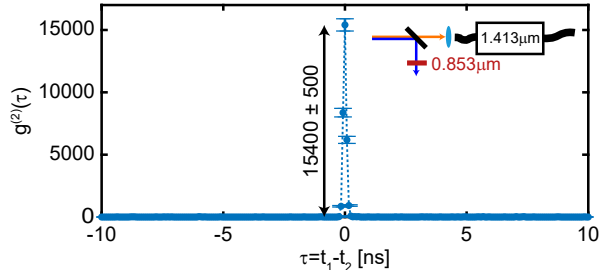


FIG. 8. Second order correlation function for low pump power coupled to the SCF device and a bandpass filter in front of the signal photon detector, and the monochromator for the idler photons set to the conjugate wavelength of the bandpass.

-
- [1] E. Ortiz-Ricardo, C. Bertoni-Ocampo, Z. Ibarra-Borja, R. Ramirez-Alarcon, D. Cruz-Delgado, H. Cruz-Ramirez, K. Garay-Palmett, and A. B. U'Ren, Spectral tunability of two-photon states generated by spontaneous four-wave mixing: fibre tapering, temperature variation and longitudinal stress, *Quantum Science and Technology* **2**, 034015 (2017).
 - [2] L. Fu, B. K. Thomas, and L. Dong, Efficient supercontinuum generations in silica suspended core fibers, *Optics Express* **16**, 19629 (2008).
 - [3] A. S. Webb, Suspended-core holey fiber for evanescent-field sensing, *Optical Engineering* **46**, 010503 (2007).
 - [4] A. M. Cubillas, S. Unterkofler, T. G. Euser, B. J. M. Etzold, A. C. Jones, P. J. Sadler, P. Wasserscheid, and P. St.J. Russell, Photonic crystal fibres for chemical sensing and photochemistry, *Chem. Soc. Rev.* **42**, 8629 (2013).
 - [5] J. P. Pocholle, J. Raffy, M. Papuchon, and E. Desurvire, Raman and four photon mixing amplification in single mode fibers, *Opt. Eng.* **24**, 600 (1985).
 - [6] J. Hansryd, P. Andrekson, M. Westlund, J. Li, and P.-O. Hedekvist, Fiber-based optical parametric amplifiers and their applications, *IEEE Journal of Selected Topics in Quantum Electronics* **8**, 506 (2002).

- [7] X. Li, J. Chen, P. Voss, J. Sharping, and P. Kumar, All-fiber photon-pair source for quantum communications: Improved generation of correlated photons, *Optics Express* **12**, 3737 (2004).
- [8] H. Takesue and K. Inoue, Generation of polarization-entangled photon pairs and violation of bell's inequality using spontaneous four-wave mixing in a fiber loop, *Phys. Rev. A* **70**, 031802 (2004).
- [9] J. G. Rarity, J. Fulconis, J. Duligall, W. J. Wadsworth, and P. St.J. Russell, Photonic crystal fiber source of correlated photon pairs, *Optics Express* **13**, 534 (2005).
- [10] J. Fan, A. Migdall, and L. J. Wang, Efficient generation of correlated photon pairs in a microstructure fiber, *Optics Letters* **30**, 3368 (2005).
- [11] B. J. Smith, P. Mahou, O. Cohen, J. S. Lundeen, and I. A. Walmsley, Photon pair generation in birefringent optical fibers, *Optics Express* **17**, 23589 (2009).
- [12] J.-H. Kim, Y. S. Ihn, Y.-H. Kim, and H. Shin, Photon-pair source working in a silicon-based detector wavelength range using tapered micro/nanofibers, *Opt. Lett.* **44**, 447 (2019).
- [13] A. A. Shukhin, J. Keloth, K. Hakuta, and A. A. Kalachev, Heralded single photon and correlated photon pair generation via spontaneous four-wave mixing in tapered optical fibers (2019), arXiv:1910.12918 [quant-ph].
- [14] M. A. Finger, T. S. Iskhakov, N. Y. Joly, M. V. Chekhova, and P. St.J. Russell, Raman-Free, Noble-Gas-Filled Photonic-Crystal Fiber Source for Ultrafast, Very Bright Twin-Beam Squeezed Vacuum, *Phys. Rev. Lett.* **115**, 143602 (2015).
- [15] M. A. Finger, N. Y. Joly, P. S. J. Russell, and M. V. Chekhova, Characterization and shaping of the time-frequency schmidt mode spectrum of bright twin beams generated in gas-filled hollow-core photonic crystal fibers, *Phys. Rev. A* **95**, 053814 (2017).
- [16] M. Cordier, A. Orioux, B. Debord, F. Gérome, A. Gorse, M. Chafer, E. Diamanti, P. Delaye, F. Benabid, and I. Zaquine, Active engineering of four-wave mixing spectral correlations in multiband hollow-core fibers, *Opt. Express* **27**, 9803 (2019).
- [17] W. J. Wadsworth, N. Joly, J. C. Knight, T. A. Birks, F. Biancalana, and P. St.J. Russell, Supercontinuum and four-wave mixing with q-switched pulses in endlessly single-mode photonic crystal fibres, *Opt. Express* **12**, 299 (2004).
- [18] R. Pennetta, S. Xie, F. Lenahan, M. Mridha, D. Novoa, and P. St.J. Russell, Fresnel-reflection-free self-aligning nanospike interface between a step-index fiber and a hollow-core photonic-crystal-fiber gas cell, *Phys. Rev. Appl* **8**, 014014 (2017).

- [19] See supplemental materials: estimation of the parametric gain, polarization dependence of the phase matching, origin of the shape of the emission spectrum, experimental implementation of the mini-cell and measurement of high CAR, .
- [20] G. Agrawal, *Nonlinear Fiber Optics*, fifth edition ed. (Academic Press, 2012).
- [21] J. Hammer, A. Cavanna, R. Pennetta, M. V. Chekhova, P. St.J. Russell, and N. Y. Joly, Dispersion tuning in sub-micron tapers for third-harmonic and photon triplet generation, *Optics Letters* **43**, 2320 (2018).
- [22] S. C. Warren-Smith, M. Chemnitz, H. Schneidewind, R. Kostecki, H. Ebendorff-Heidepriem, T. M. Monro, and M. A. Schmidt, Nanofilm-induced spectral tuning of third harmonic generation, *Optics Letters* **42**, 1812 (2017).
- [23] The seemingly high fluctuations in this region are due to the low count rates for these time bins.
- [24] Y. M. Mikhailova, P. A. Volkov, and M. V. Fedorov, Biphoton wave packets in parametric down-conversion: Spectral and temporal structure and degree of entanglement, *Physical Review A* **78**, 062327 (2008).
- [25] G. Brida, V. Caricato, M. V. Fedorov, M. Genovese, M. Gramegna, and S. P. Kulik, Characterization of spectral entanglement of spontaneous parametric-down conversion biphotons in femtosecond pulsed regime, *EPL (Europhysics Letters)* **87**, 64003 (2009).
- [26] M. Liscidini and J. E. Sipe, Stimulated Emission Tomography, *Physical Review Letters* **111**, 193602 (2013).
- [27] B. Fang, O. Cohen, M. Liscidini, J. E. Sipe, and V. O. Lorenz, Fast and highly resolved capture of the joint spectral density of photon pairs, *Optica* **1**, 281 (2014).
- [28] A. W. Snyder and J. D. Love, *Optical Waveguide Theory* (Springer US, 1983).